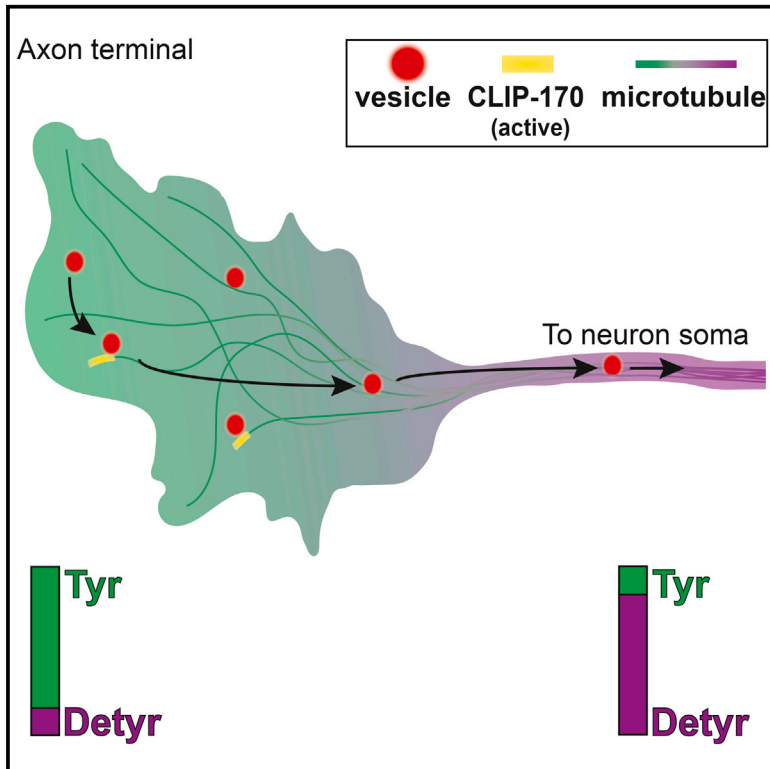# α-Tubulin Tyrosination and CLIP-170 Phosphorylation Regulate the Initiation of Dynein-Driven Transport in Neurons

Graphical Abstract

Authors

Jeffrey J. Nirschl, Maria M. Magiera, Jacob E. Lazarus, Carsten Janke, Erika L.F. Holzbaur

Correspondence

holzbaur@mail.med.upenn.edu

In Brief

Nirschl et al. use in vitro reconstitution assays and live-cell imaging of cultured neurons to show that a tyrosinated α-tubulin gradient provides spatial regulation whereas CLIP-170 phosphorylation allows spatiotemporal modulation of retrograde transport initiation.

Highlights

- CLIP-170 phosphorylation regulates transport initiation in vitro and in neurons

- α-Tubulin tyrosination enhances the efficiency of cargo binding to microtubules

- Dynactin on neuronal vesicles mediates binding to CLIP-170 and tyrosinated α-tubulin

- Transport initiation in neurons fits a regulated diffusive search-and-capture model

CellPress

Article

α-Tubulin Tyrosination and CLIP-170 Phosphorylation Regulate the Initiation of Dynein-Driven Transport in Neurons

Jeffrey J. Nirschl,[1] Maria M. Magiera,[2,3] Jacob E. Lazarus,[1] Carsten Janke,[2,3] and Erika L.F. Holzbaur[1,*]
[1]Department of Physiology, Perelman School of Medicine, University of Pennsylvania, Philadelphia, PA 19104, USA
[2]Institut Curie, PSL Research University, CNRS UMR3348, 91405 Orsay, France
[3]Université Paris Sud, Université Paris-Saclay, CNRS UMR3348, 91405 Orsay, France
*Correspondence: holzbaur@mail.med.upenn.edu
http://dx.doi.org/10.1016/j.celrep.2016.02.046

SUMMARY

Motor-cargo recruitment to microtubules is often the rate-limiting step of intracellular transport, and defects in this recruitment can cause neurodegenerative disease. Here, we use in vitro reconstitution assays with single-molecule resolution, live-cell transport assays in primary neurons, computational image analysis, and computer simulations to investigate the factors regulating retrograde transport initiation in the distal axon. We find that phosphorylation of the cytoskeletal-organelle linker protein CLIP-170 and post-translational modifications of the microtubule track combine to precisely control the initiation of retrograde transport. Computer simulations of organelle dynamics in the distal axon indicate that while CLIP-170 primarily regulates the time to microtubule encounter, the tyrosination state of the microtubule lattice regulates the likelihood of binding. These mechanisms interact to control transport initiation in the axon in a manner sensitive to the specialized cytoskeletal architecture of the neuron.

INTRODUCTION

Microtubule-based transport by molecular motors is essential in most eukaryotic cells. One of the first steps in transport is to recruit motor-cargo complexes to microtubules. This process can be regulated at multiple levels, including the motor, motor adaptors, microtubule associated proteins (MAPs), or the microtubule track itself. How the cell integrates these multiple layers of regulation to allow precise spatial and temporal control of transport initiation is not yet understood.

The specialized morphology of neurons renders these cells particularly dependent on the precise regulation of transport initiation. Due to the uniform plus-end-out orientation of microtubules in the axon, the dynein-dynactin complex is the primary motor driving retrograde transport from the distal axon toward the cell soma. Efficient loading of dynein-dynactin-bound cargos is crucial for neuronal survival, as mutations in dynein or dynactin

cause neurodegeneration in mice and humans (Maday et al., 2014). More specifically, mutations in the highly conserved cytoskeleton-associated protein glycine-rich (CAP-Gly) domain of the p150[Glued] subunit of dynactin cause a significant reduction of retrograde transport initiation in neurons in vitro and in vivo (Moughamian and Holzbaur 2012; Lloyd et al., 2012). In humans, mutations in the CAP-Gly domain of dynactin are sufficient to cause a lethal form of parkinsonism known as Perry syndrome (Farrer et al., 2009).

The mechanisms controlling the initiation of retrograde transport involve plus-end binding proteins or +TIPs (Akhmanova and Steinmetz, 2008) including CLIP-170 (CLIP1), p150[Glued] (DCTN1), and end binding proteins EB1 or EB3 (MAPRE1 or MAPRE3), collectively referred to as EBs (Moughamian and Holzbaur, 2012; Moughamian et al., 2013). Dynein is thought to be dynamically recruited to the microtubule plus end via hierarchical interactions of EBs, CLIP-170, and p150[Glued] (Ayloo et al., 2014; Bieling et al., 2008; Dixit et al., 2009; Duellberg et al., 2014; Lomakin et al., 2009; Moughamian et al., 2013; Watson and Stephens, 2006) (Figure 1A). Although many of the molecular players in this pathway are known, how this recruitment pathway is regulated in neurons is not understood.

CLIP-170 may serve as one crucial regulatory point, as this protein can link p150[Glued] to EBs, and CLIP-170 binding interactions are regulated by phosphorylation (Rickard and Kreis, 1991; Lee et al., 2010). CLIP-170, the first identified +TIP, was initially characterized as a cytoplasmic linker between endosomes and microtubules (Pierre et al., 1992; Rickard and Kreis, 1996). CLIP-170 can assume a folded, autoinhibited conformation when phosphorylated in the third serine-rich domain or an open conformation when dephosphorylated (Lansbergen et al., 2004; Lee et al., 2010). These observations led to the hypothesis that CLIP-170 phosphorylation may provide a way to dynamically regulate recruitment of vesicular cargo to microtubules; however, direct evidence for this model in neurons is lacking.

Post-translational modifications of the microtubule track are another potential mechanism to regulate the recruitment of microtubule motors (Wehenkel and Janke, 2014; Yu et al., 2015). In neurons, there is a spatial gradient of tubulin modifications along both axons and dendrites (Janke and Kneussel, 2010). Intriguingly, the retrograde transport initiation zone in the distal axon defined by live-cell imaging (Moughamian and
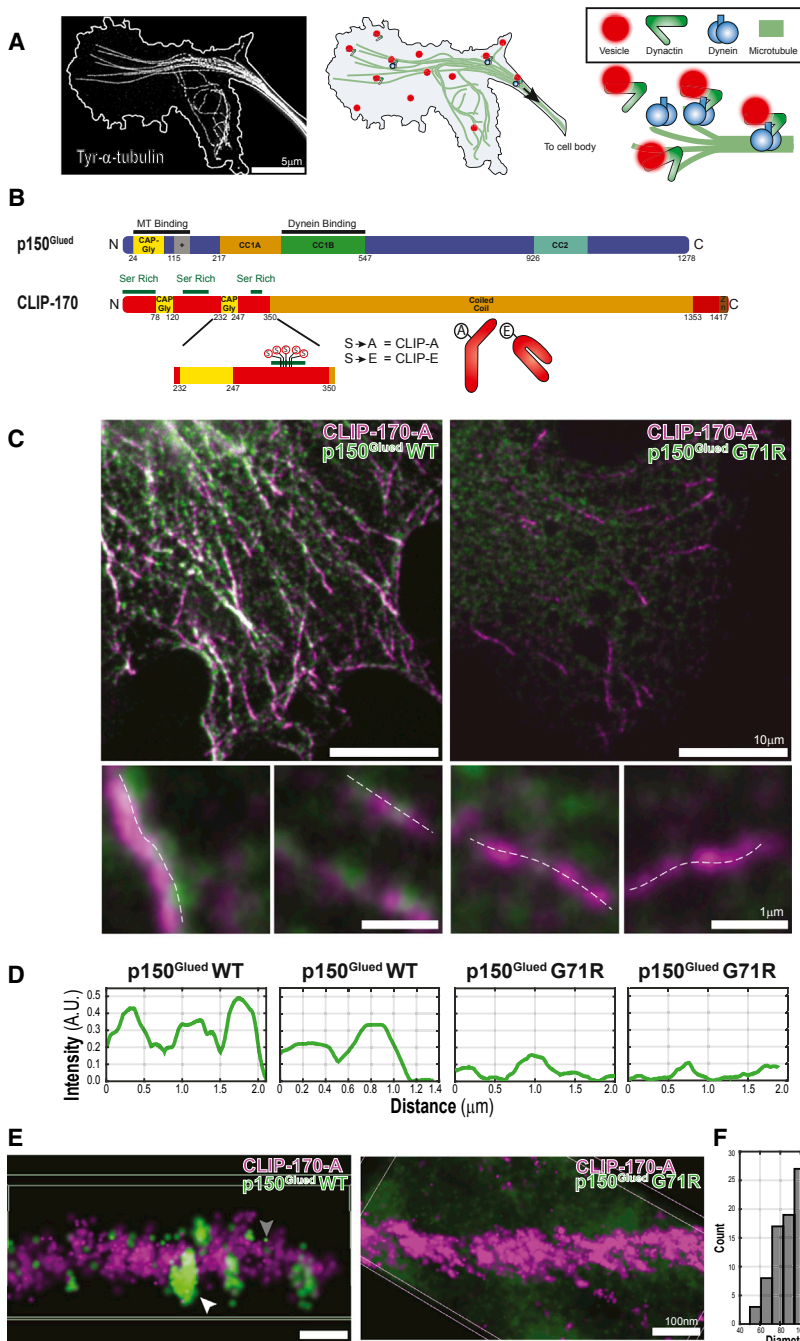
(A) Deconvolved maximum projection STED image of microtubules in the neuronal growth cone with the cell border outlined in white (left). Schematic of the recruitment of dynein-dynactin organelles in the neuronal growth cone (right).

(B) Schematic of p150[Glued] (above) showing the CAP-Gly, basic (+), and coiled-coil domains. Schematic of CLIP-170 with relevant CAP-Gly, Ser rich, coiled-coil, and Zinc knuckle (Zn) domains. The phosphorylation sites S-309, 311, 313, 319, and 320 and phosphomutant constructs are shown below.

(C) Confocal slices of COS-7 cells co-transfected with HT-CLIP-A and either full-length myc-p150[Glued] WT or G71R (top row). Upsampled images of individual comets show punctate p150[Glued] associated with CLIP-A comets (below). The dashed white lines denote where line profiles were performed in (D).

(D) Line intensity profiles along upsampled images in (C).

(E) 3D-STORM super-resolution was used to image microtubules in fixed COS-7 cells (Movie S1). Shown are cropped microtubule plus ends from the two different conditions. CLIP-A (magenta) fully decorates the plus end as comet-like structures, and discrete p150[Glued] clusters associate with the CLIP-A comet (tubulin is unlabeled in these images). This shows that p150[Glued] forms discrete punctate structures (white arrowhead) on CLIP-A comets; the morphology of these punctae is consistent with a vesicular population. In addition, there is a separate population of point-localized individual p150[Glued] molecules (gray arrowhead).

(F) Histogram of the maximum equatorial diameter for ellipses manually fit around clusters of p150[Glued] WT puncta in STORM images (n = 133 puncta total from two cells, N = 1).

Both CLIP-170 and p150[Glued] are sensitive to the C-terminal tyrosine motif of Tyr-α-tubulin (Peris et al., 2006; Bieling et al., 2008), suggesting that this modification may play a role in spatially defining retrograde transport initiation in the distal axon, although this hypothesis has not been tested.

Here, we address the regulation of transport initiation using both in vitro reconstitution of organelle binding to microtubules and live-cell assays in primary neurons. We find that the phosphodeficient, open conformation of CLIP-170 effectively promotes transport initiation in vitro and in neurons. We also find that isolated neuronal vesicles, in complex with motors/adaptors, show a robust preference for Tyr-microtubules over Detyr-microtubules. These mechanisms interact, as CLIP-170 phosphorylation levels further modulate motor-cargo recruitment to Tyr-microtubules. Together, our observations fit a multi-modal recruitment model, where both the microtubule modification status and CLIP-170

Holzbaur, 2012) coincides with a region enriched for tyrosinated (Tyr) α-tubulin (Robson and Burgoyne, 1989; Brown et al., 1993). Most α-tubulins are initially synthesized with a C-terminal EEY motif, but the terminal tyrosine of this motif can be cleaved by a tyrosine carboxypeptidase following assembly of tubulin dimers into the microtubule lattice (Kumar and Flavin, 1981). The cleavage of the terminal tyrosine to form detyrosinated α-tubulin (Detyr) can only be reversed following disassembly of the microtubule, as the enzyme tubulin tyrosine ligase (TTL) acts on soluble Detyr tubulin dimers (Ersfeld et al., 1993; Prota et al., 2013).

phosphorylation specifically tune the kinetics of transport initiation to the requirements of the cell. Computer simulations of organelle dynamics in the distal axon indicate that CLIP-170 primarily regulates the time to microtubule encounter, while the tyrosination state of tubulin regulates the likelihood of binding. Together, these mechanisms provide spatiotemporal specificity, with spatial regulation controlled by the distal gradient of Tyr-microtubules and temporal regulation via control of the phosphorylation state of CLIP-170.

RESULTS

CLIP-170 Comets Serve as Docking Sites for p150[Glued] Vesicles in Cells

Conformational changes in CLIP-170 regulate its association with microtubules and the accessibility of the C terminus for binding to other +TIPs (Lansbergen et al., 2004). Phosphomimetic mutations in the third serine-rich domain of CLIP-170 promote a closed, autoinhibited conformation, while phosphodeficient mutations promote an open conformation (Lee et al., 2010). We generated phosphomimetic (CLIP-E) and phosphodeficient (CLIP-A) constructs by mutating five key serine residues to Ala or Glu, respectively (Figure 1B), and confirmed previous observations (Lee et al., 2010), using confocal microscopy to show that CLIP-A decorates microtubule plus end as comets that are significantly longer than CLIP-E comets (Figures S1A and S1B). The C-terminal zinc knuckle and EEY motif of CLIP-170 are exposed in phosphodeficient CLIP-A; these motifs can recruit dynactin through a direct interaction with the p150[Glued] subunit (Galjart, 2005; Duellberg et al., 2014). Co-expression of CLIP-A with myc-tagged p150[Glued] induces the pronounced localization of p150[Glued]-positive puncta to CLIP-170 comets (Figures 1C and 1D). The resulting linear punctate arrays are reminiscent of vesicles binding to microtubules (Gill et al., 1991; Vaughan et al., 1999). As in vitro studies have shown that the CAP-Gly domain of p150[Glued] binds directly to CLIP-170 (Weisbrich et al., 2007), we tested whether the localization of p150[Glued] puncta to CLIP-170 comets was dependent on this interaction by comparing the localization of wild-type p150[Glued] to that of a G71R point mutation in the CAP-Gly domain. This mutation is causative for the lethal neurodegenerative disease known as Perry syndrome (Farrer et al., 2009) and acts as a loss-of-function mutation for the CAP-Gly domain (Moughamian and Holzbaur, 2012). As shown in Figures 1C and 1D, the recruitment of myc-tagged p150[Glued]-positive puncta to CLIP-A comets observed in cells expressing wild-type p150[Glued] was abolished in cells expressing similar levels (Figure S1C) of the G71R point mutation.

To better visualize the population of p150[Glued]-positive puncta in cells, we used direct stochastic optical reconstruction microscopy (dSTORM) super-resolution microscopy. This approach more clearly revealed discrete clusters of localized p150[Glued] associated with CLIP-A comets (Figures 1E and S1D; Movie S1). Using dSTORM, we measured the size distribution of p150[Glued]-positive puncta and found a mean diameter of 103 ± 2 nm (Figure 1F); parallel analysis on stimulated emission depletion (STED)-acquired images resulted in an average diameter of 106 ± 3 nm. These measurements are very similar to the 90-nm diameter determined for isolated dynactin-positive neuronal vesicles as measured by electron microscopy (Hendricks et al., 2010). Thus, a population of p150[Glued]-positive vesicles dock at CLIP-170 comets in cells; this docking requires an intact CAP-Gly domain.
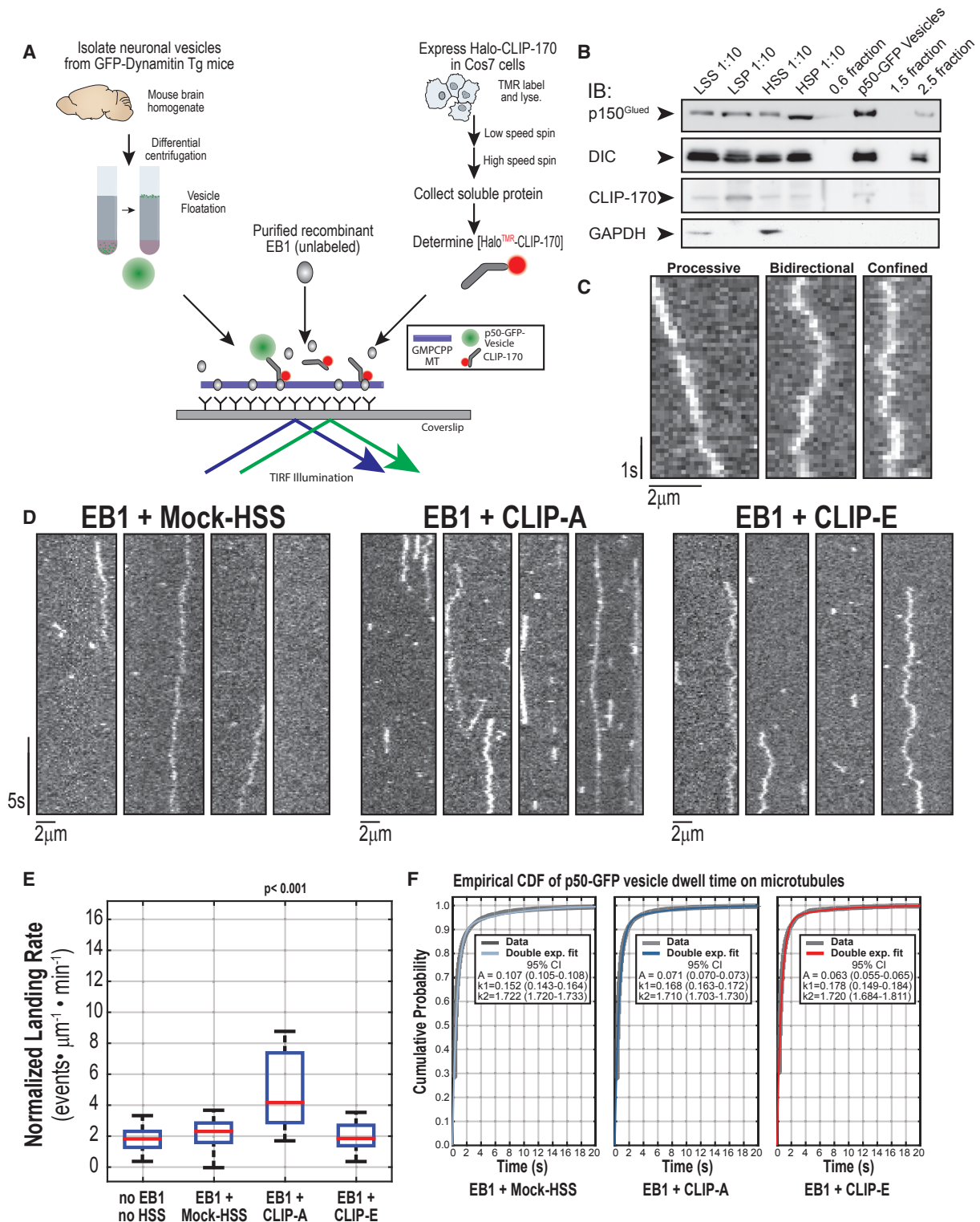
Reconstitution of CLIP-170-Dependent Organelle Recruitment In Vitro

To study the regulation of organelle recruitment by CLIP-170 phosphorylation at the single-molecule level, we moved to an in vitro system using neuronal vesicles isolated from the brains of p50-EGFP transgenic mice (Ross et al., 2006; Hendricks et al., 2010) visualized with single-molecule total internal fluorescence (TIRF) microscopy. Vesicles co-purify with an endogenous complement of dynein, dynactin, and kinesins (Figure S2); are positive for markers of late-endosomes/lysosomes (Rab7/LAMP-1), but not early endosomes (Rab5); and exhibit dynein-dependent motility in vitro (Hendricks et al., 2010). To mimic recruitment of organelles to the GTP-like microtubule lattice at the plus end, we used guanosine-5′-[(α,β)-methyleno]triphosphate (GMPCPP) stabilized microtubules (Alushin et al., 2014) that specifically recruit +TIPs including EB1 and CLIP-170 (Dixit et al., 2009; Zanic et al., 2009; Lopez and Valentine, 2015) and provide a stable landing platform more tractable for automated analysis of landing rates than dynamic microtubules. To this, we added purified recombinant unlabeled EB1 and high-speed supernatant (HSS) from COS-7 cells transfected with either HaloTag (HT) CLIP-A or CLIP-E or HSS from mock-transfected cells (Mock-HSS) (Figure 2A). As endogenous CLIP-170 is not enriched in our vesicle population (Figure 2B), it likely functions as a cytosolic accessory factor. To ensure equal levels of HT-CLIP in the assay, we measured the absorbance of the tetramethylrhodamine (TMR)-labeled protein (Figures S3A and S3B); HT-CLIP levels were further confirmed by western blotting (Figure S3C).

To analyze landing rates of vesicles loading onto microtubules, we applied unbiased, whole-field, multi-particle tracking using uTrack software (Jaqaman et al., 2008) to track particles, map their starting coordinates to microtubule masks and measure landing rates and dwell times (Figure S3F). Representative kymographs of p50-GFP-vesicles show processive, bidirectional, or confined motility, defined by mean squared displacement (Figure 2C). p50-GFP-vesicles with EB1 in the absence of exogenous CLIP-170 show a low, basal rate of microtubule landing (Figure 2D). In the presence of EB1+CLIP-A, vesicles show a 2-fold enhancement of the landing rate, an effect not seen in any other condition (Figure 2E). Importantly, however, dwell times were not significantly different among conditions, suggesting that the increased recruitment induced by CLIP-A does not affect the characteristic dwell time of the motor-cargo complex (Figure 2F).

CLIP-170 Phosphorylation State Modulates Retrograde Transport Initiation in Neurons

Next, we used live-cell imaging of primary dorsal root ganglion (DRG) sensory neurons to test whether the phosphorylation state of CLIP-170 regulates retrograde transport in the distal axon (Moughamian and Holzbaur 2012). We depleted endogenous

Figure 2. Reconstitution of CLIP-170-Dependent Organelle Recruitment In Vitro

(A) Schematic of in vitro reconstitution assay with p50-GFP-vesicles, EB1, and CLIP-A or CLIP-E in COS-7 cell extract HSS.

(B) Western blot of fractions from neuronal vesicle isolation from mouse brain shows p150[Glued] and DIC are enriched in the vesicle fraction. Most of the CLIP-170 is retained in the low-speed pellet, and only a faint band for endogenous CLIP-170 is found in the vesicle fraction. Cytosolic marker GAPDH is not enriched in the vesicle fraction.

(legend continued on next page)

CLIP-170 using small interfering RNA (siRNA) and expressed siRNA-resistant wild-type (WT) or phosphomutant forms of CLIP-170. To visualize retrograde transport, we also expressed LAMP-1-RFP. To unambiguously measure retrograde transport initiation, we photobleached a 40-μm region of axon 10 μm proximal to the distal growth cone tip, then measured the flux of LAMP-1-RFP organelles moving in the retrograde direction from the growth cone into the bleached region (Figure 3A). CLIP-170 knockdown reduces distal initiation (Figure 3B). As previously noted, the effect of CLIP-170 knockdown on distal initiation is specific, as it does not significantly alter retrograde flux along the mid-axon (Moughamian et al., 2013). Quantitative analysis of Oregon-green-labeled CLIP rescue constructs demonstrated that all expressed to similar levels (Figure S4), but strikingly, only expression of either CLIP-WT or CLIP-A was capable of rescuing transport initiation to normal levels following CLIP-170 knockdown. In contrast, CLIP-E only partially rescued the deficit caused by loss of endogenous CLIP-170 expression (Figures 3B and 3C; Table S1). Importantly, the number of vesicles in the growth cone was comparable across all conditions, indicating that the decreased flux observed in the knockdown and CLIP-E rescue experiments was not due to depletion of the distal vesicle pool, nor do we see a deficit in anterograde transport (Figure 3D). Thus, consistent with our in vitro results, the phosphorylation state of CLIP-170 modulates retrograde transport initiation in neurons.

The Distal Axon Is Rich in Tyrosinated α-Tubulin

The retrograde transport initiation zone observed in our live-cell experiments is coincident with the region of the distal axon thought to be enriched for tyrosinated α-tubulin (Robson and Burgoyne, 1989; Brown et al., 1993). We used super-resolution imaging to more precisely map the tyrosination state of α-tubulin along the axon. STED imaging of the distal axon of cultured DRG neurons shows a profound enrichment of Tyr-tubulin over Detyr-tubulin distally (Figures 4A and 4B). We measured the Tyr/Detyr gradient, which stretches ∼20 μm from the axon tip and then decreases moving proximally toward the cell body (Figure 4C). This gradient correlates spatially with the distal loading zone observed in live-cell assays, and in conjunction with previous observations that p150[Glued] puncta preferentially localize to tyrosinated microtubules in nonpolarized cells (Vaughan et al., 1999; Peris et al., 2006), this led us to test the contribution of Tyr-microtubules to organelle recruitment.

Tyrosinated α-Tubulin Promotes Robust Organelle Recruitment In Vitro

We directly compared the recruitment of organelles to Tyr- and Detyr-microtubules using an in vitro reconstitution assay (Figure 5A). Tubulin purified from HeLa cells is primarily tyrosinated; brief treatment with carboxypeptidase A (CPA) produces a population highly enriched in Detyr tubulin (Figure 5B) (Barisic et al., 2015; Kreitzer et al., 1999). Microtubules were polymerized from either Tyr- or Detyr-tubulin and GMPCPP and differentially labeled with AF-647- and TRITC-conjugated tubulin at a low ratio (5%); there was no significant difference in length between Tyr- and Detyr-microtubules (Figure S5A). Labeled Tyr- and Detyr-microtubules were flowed into the same chamber, allowing the simultaneous measurement of landing rates.

Kymographs of interactions of p50-GFP-vesicles with Detyr-microtubules show a low basal landing rate (Figure 5C), similar to landing rates observed with microtubules polymerized from bovine brain tubulin (Figure 2E). In contrast, we observed a more than 4-fold increase in the landing of p50-GFP vesicles onto Tyr-microtubules (Figure 5D; Movie S2). The choice of fluorescent label did not affect our observations, as the reversing the labels on Tyr-/Detyr-microtubules did not affect the results (Figures S5B–S5D; Movie S3). Importantly, we found that despite the marked differences in landing rates, dwell times for vesicles bound to either Tyr- or Detyr-microtubules were very similar. Thus, the mechanisms that promote recruitment to the microtubule are distinct from the processes that determine the sustained engagement of the motor-cargo complex.

CLIP-170 Phosphorylation Regulates Recruitment to Tyr-Microtubules

CLIP-170, with two tandem CAP-Gly domains per monomer (four per dimer complex), is also sensitive to Tyr-tubulin, and preferential recruitment of CLIP-170 to Tyr-microtubules has been shown in cells and in vitro (Peris et al., 2006; Bieling et al., 2008). However, it is not known how phosphorylation affects the binding of CLIP-170 to Tyr-tubulin. Using single-molecule TIRF microscopy, we measured the landing rates on Tyr-/Detyr-microtubules for TMR-HT-labeled CLIP-WT, CLIP-A, and CLIP-E expressed in cell lysates. Constitutively active kinesin-1 motor domain fused to a TMR-HT (CA-kinesin-1[560]) was used as a control; we saw robust localization to both Tyr- and Detyr microtubules.

Maximum intensity projection images over time show colocalization of CLIP-WT and CLIP-A with Tyr-microtubules but little binding to Detyr-microtubules (Figure 6A). CLIP-E was recruited poorly to either Tyr- or Detyr-microtubules. Quantification of

---

(C) Representative kymographs of p50-GFP-vesicles on GMPCPP microtubules show that they exhibit processive, bidirectional, and confined motility, as defined by mean squared displacement analysis of particle trajectories.

(D) Representative kymographs of p50-GFP-vesicles on single GMPCPP microtubules from each of the three conditions (100 nM EB1 + mock-HSS or CLIP-A or CLIP-E in motility assay buffer). The estimated final concentration of TMR-labeled HT-CLIP in this assay was ∼100 nM. EB1 + mock-HSS and EB1 + CLIP-E show a basal landing rate, whereas there is an increase in organelle recruitment with CLIP-A. At least three different preparations of cell lysates were used.

(E) Quantification of the landing rates in each of the experimental conditions shows a significant increase in organelle recruitment only with EB + CLIP-A (n > = 22 movies per condition with each movie with >500 events per movie; N > = 3 independent vesicle isolations; Kruskal-Wallis [KW] one-way ANOVA with Tukey post-tests).

(F) Empirical cumulative distribution function (CDF) for microtubule dwell times of all non-fixed particles. The stair plot starts at 0.1 s, as this is the minimum observable dwell time. Double exponential fit obtained via maximum likelihood estimation (MLE) with 100 bootstrapped fits to obtain 95% CI. The dwell time distributions for mock-HSS, CLIP-A, and CLIP-E were compared in pairs using a two-sample Kolmogorov-Smirnov (KS) test with a Bonferroni correction (p > 0.20 for all comparisons; n > 1,500 particles per condition; N > = 3).
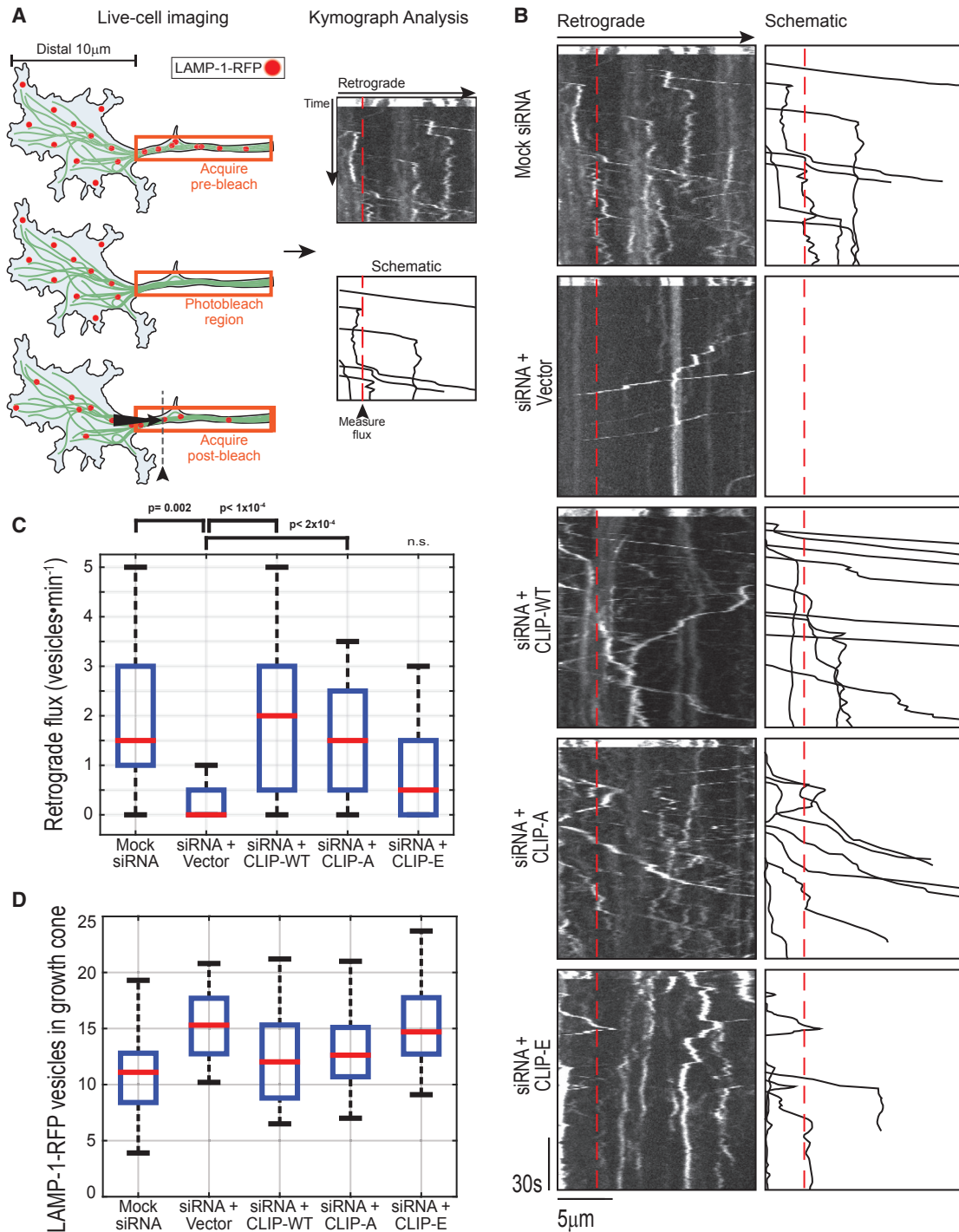
Figure 3. CLIP-170 Phosphorylation State Modulates Retrograde Transport Initiation in Neurons

(A) Schematic of live-cell assay for retrograde transport initiation in neurons.

(B) Representative kymographs for each condition with a schematic tracing of the analyzed vesicles to the right. The dashed red line indicates 3.5 μm from the distal end of the bleaching region of interest and is the site for flux analysis.

(C) Quantification of retrograde flux for all conditions. CLIP-170 knockdown reduces the efficiency of retrograde flux, and this is rescued by CLIP-WT or CLIP-A, but CLIP-E shows incomplete rescue (n = 18–36 neurons total, N > 3 experiments; KW ANOVA with Tukey post-tests). A complete list of the pairwise post-tests is shown in Table S1.

(D) Quantification of the number of LAMP-1-RFP vesicles in the growth cone at the start of the movie shows a comparable distribution of vesicles indicating that the reduced retrograde flux in the siRNA or siRNA + CLIP-E is not due to a reduced distal vesicle pool.

landing rates confirms that CLIP-WT and CLIP-A show a significant preference for Tyr-microtubules (Figure 6B; Table S2). Although CLIP-E retains a significant preference for Tyr, its landing rate is significantly reduced relative to CLIP-WT or CLIP-A (Table S2). The landing rates for CA-kinesin-1[560] were similar on both Tyr- or Detyr-microtubules, confirming that sensitivity to Tyr-microtubules is not a general feature of microtubule binding proteins in this assay.

p150[Glued] CAP-Gly Is a Major Factor on Vesicles for Sensing Tyr-α-Tubulin

To further define the domains involved in recruitment, we tested the specificity of purified recombinant constructs of CLIP-170 and p150[Glued] (Figure S6) for binding to Tyr- and Detyr-microtubules, in comparison to the motor domain of kinesin-1. We find that the N-terminal H2 fragment of CLIP-170 and the N terminus of p150[Glued] [1–210] are both robustly sensitive to the tyrosination state of the microtubules (Figures 6C and 6D), consistent with previous results (Peris et al., 2006; Bieling et al., 2008). Importantly, we find that the ability of p150[Glued] to sense tubulin tyrosination requires only the CAP-Gly domain, as deletion of the low-microtubule-affinity basic domain does not reduce the preference for Tyr-microtubules, while deletion of the CAP-Gly completely abolishes microtubule binding (Figure 6C). Of the potential CAP-Gly proteins sensitive to tubulin tyrosination that we tested, only p150[Glued] is selectively enriched in our vesicle fraction (Figure 2B). In previous work, we have shown that the CAP-Gly domain of p150[Glued] is the major determinant mediating the initial interaction of neuronal vesicles with the microtubule, as vesicle binding is effectively blocked by pre-incubation with a monoclonal antibody specific for this domain, but not by antibodies to dynein or kinesin motors (Hendricks et al., 2010). Thus, we conclude that the CAP-Gly domain of p150[Glued] is likely the major determinant regulating the specificity of neuronal vesicles for tyrosinated microtubules.

Simulation of Vesicle Diffusion and Microtubule Capture in the Distal Axon

Our experimental data indicate that both the phosphorylation state of CLIP-170 and the tyrosination state of the microtubule contribute to effective cargo capture. To rigorously test our model, we performed Monte-Carlo simulation of vesicle diffusion and microtubule capture using experimentally derived parameters. In the simulation, vesicles initiate at random positions in the growth cone and undergo 2D diffusion until they reach the microtubule, upon which capture occurs at a pre-specified probability. We model the open conformation of CLIP-170 as an extended ~135-nm rod (Scheel et al., 1999) that can increase the effective microtubule search radius when bound to the lattice. We simulated two extremes, one where CLIP-170 does not decorate the microtubule as a model for CLIP-E and a second scenario assuming full microtubule decoration as model for CLIP-A, simulated by dilating the microtubule mask by a disk structuring element of radius 135 nm. The tyrosination state of microtubules is incorporated into the model by altering the normalized binding probability, with binding probabilities of 1 and 0.25 for Tyr- and Detyr-microtubules, respectively, values empirically determined from vesicle landing rates on Tyr- or Detyr-microtubules (Fig-

ure 5D). To model the diffusion constant of vesicles in the cytoplasm, we used an empirically determined diffusion constant, D, of 0.006 μm^2/s (Zajac et al., 2013). However, we also performed parallel simulations over a broad range of diffusion constants. For each condition, 1,000 vesicles were randomly seeded within the growth cones of four different simulation spaces traced from experimentally captured STED images. Vesicles were allowed to diffuse for a maximum of 20 min simulated time, and the position of each vesicle was determined every 100 ms (pseudocode shown in Figure S7A). All simulations for a given condition were repeated five independent times for a total of 5,000 simulated vesicles per neuron (2 × 10^4 per condition).

CLIP-A decoration reduces the effective distance to the microtubule compared to CLIP-E, thus increasing the microtubule search radius. At a binding probability of 1 (Tyr), this dramatically reduced the effective time for microtubule capture of randomly seeded vesicles undergoing 2D diffusion (Figure 7B). The effect of CLIP-A in reducing the median time to microtubule capture holds over three orders of magnitude of diffusion constants, from 0.001 to 1.0 μm^2/s (Figures 7C and S7B). Strikingly, we found a 2.4-fold increase in the number of vesicles that never encounter a microtubule over the 20-min course of the simulation in our models of CLIP-E as compared to CLIP-A (Figure S7C). To our surprise, our modeling revealed that decreasing the binding probability to 0.25 to mimic binding to Detyr-microtubules had only a modest effect on the median time to microtubule capture (Figure 7B). We also repeated our simulation limiting CLIP-A decoration to the terminal ~2 μm of the microtubule (D = 0.006 μm^2/s). Again, we saw that CLIP-A significantly reduced the median capture time, in this case by an average of 5.0 s (95% confidence interval [CI], 4.8–5.1) as compared to CLIP-E. Finally, to test the overall utility of our model, we calculated the predicted rate of retrograde flux from our simulation. The flux rate observed in our simulation is not too far from our measured rates of flux in primary neurons, further supporting the predictive power of our modeling (Figure 7D).

Thus, both our experimental observations and our simulations are consistent with a multi-modal recruitment model, where CLIP-170 phosphorylation and the tyrosination state of microtubules regulate transport initiation via interacting pathways. The primary role of CLIP-170 is to extend the microtubule search radius, reducing diffusion times in a region of the cell characterized by sparse microtubules, while gradient of Tyr-microtubules provides spatial specificity by promoting efficient organelle recruitment.

DISCUSSION

Multi-modal Regulation of Transport Initiation

The initial recruitment of motor-cargo complexes to microtubules may be the rate-limiting step of intracellular transport, and this process is likely to be regulated for efficient, coordinated organelle motility in the cell. Here, we show that CLIP-170 phosphorylation regulates organelle transport initiation in vitro and in neurons in a mechanism dependent on the canonical plus-end tracking EB proteins. In addition, we find regulation at the level of the microtubule track, as enrichment of tyrosinated α-tubulin in the microtubule lattice also promotes robust organelle recruitment.
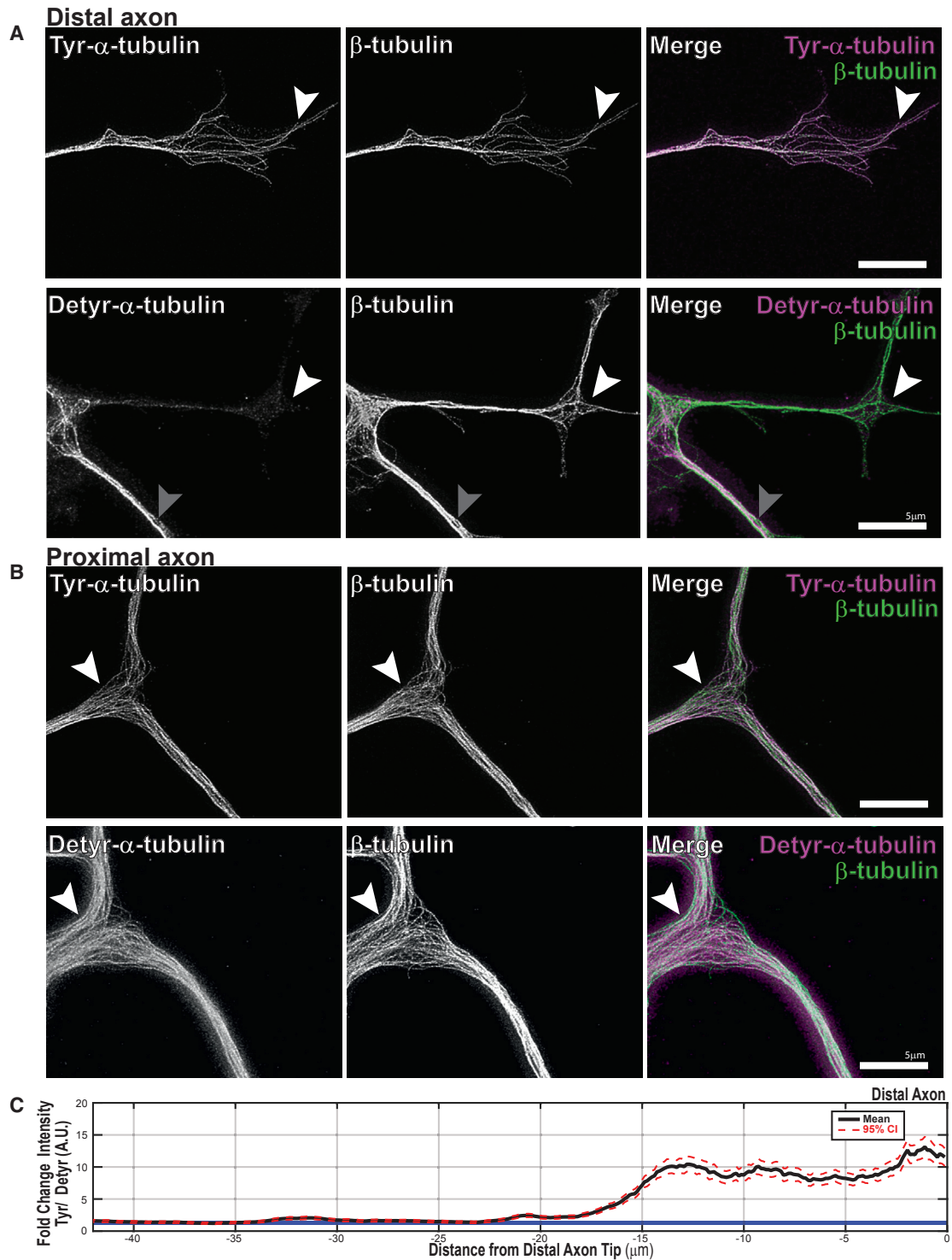
Figure 4. The Distal Axon Is Rich in Tyrosinated α-Tubulin

(A) STED super-resolution images of the distal axon shows an enrichment of tyrosinated α tubulin (white arrowhead, distal axon; gray arrowhead, ~30 μm proximal to the distal axon tip).

(B) Detyrosinated α tubulin is enriched in the proximal axon, relative to tyrosinated α tubulin. The white arrowhead shows the first axonal branch point after exiting the cell body. The cell body was identified by morphology but is not shown in these images.

(legend continued on next page)
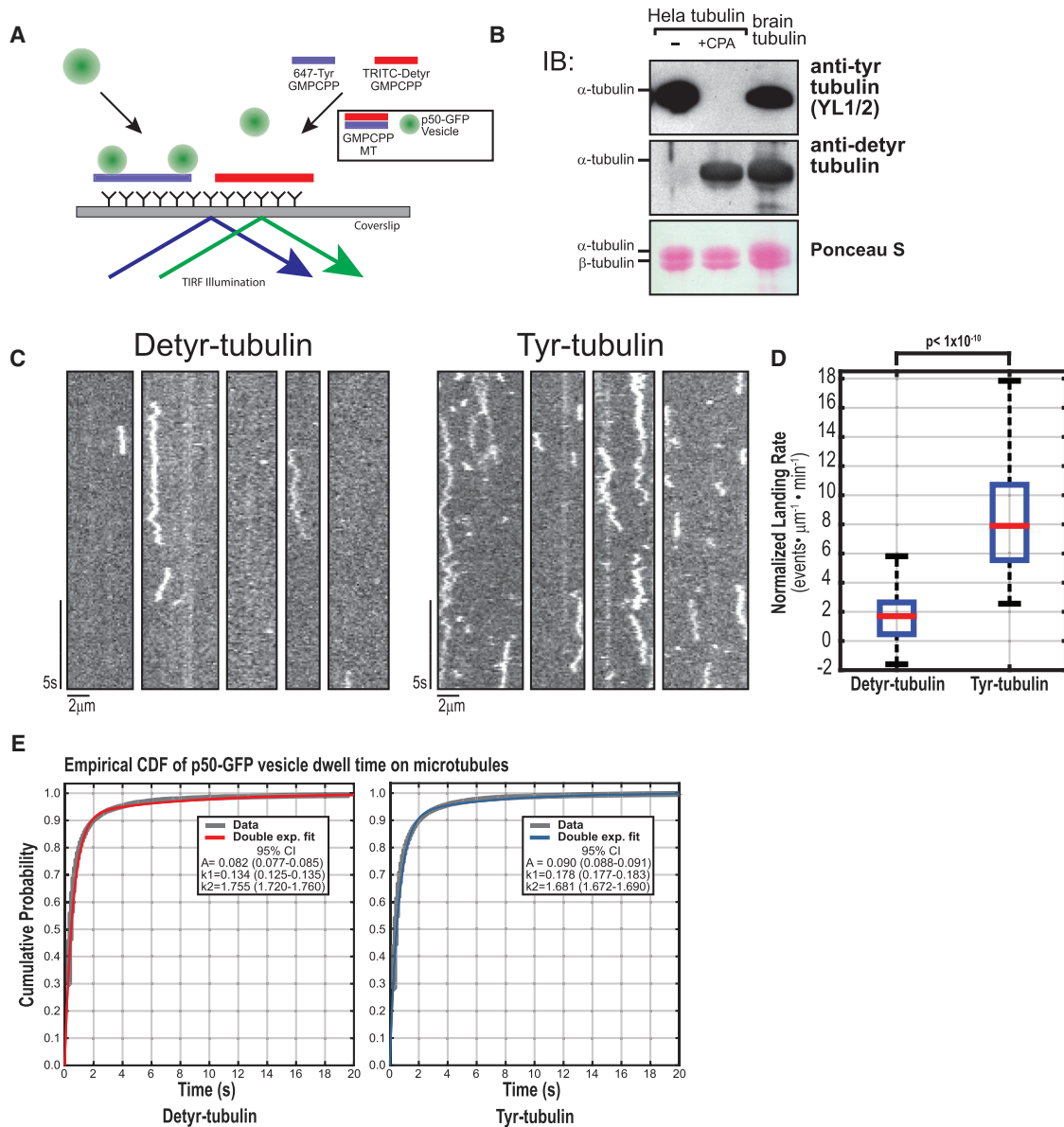
Figure 5. Tyrosinated α-Tubulin Promotes Robust Organelle Recruitment In Vitro

(A) Schematic of the p50-GFP-vesicle recruitment assay using GMPCPP stabilized Tyr-/Detyr-microtubules labeled separately with either 5% AF-647 or TRITC.

(B) Western of Tyr/ Detyr tubulin purified from HeLa cells shows a homogenous population of fully tyrosinated or fully detyrosinated tubulin, compared to brain tubulin.

(C) Representative kymographs of p50-GFP-vesicle landing on Detyr versus Tyr microtubules.

(D) Quantification of landing rate shows a robust and significant increase in landing rate on Tyr microtubules (n = 70 movies per condition, each movie with > 500 events; N = 3 independent vesicle isolations; Wilcoxon rank-sum test p < 1 × 10^{-10}).

(E) Empirical CDF for microtubule dwell times of all non-fixed particles with double exponential fit and 95% CI for fit parameters. The dwell time distributions for vesicles on Tyr or Detyr microtubules were compared using a two-sample KS test (p = 0.07; n > 1 × 10^4 particles per condition, N = 3).

Together, these results favor a multi-modal recruitment model where interacting layers of regulation promote efficient, robust, and regulated transport. Multi-modal recruitment advances the "search-capture" model for recruitment of dynein-dependent cargo (Vaughan, 2005) in at least two important ways. First, the observation that Tyr-microtubules

(C) Bootstrapped mean and 95% CI for line intensity profiles of Tyr/ Detyr in the distal axon (n = 4 neurons per condition, 10 line profiles per neuron; N = 2). The blue line indicates a ratio of 1.

The images for Tyr or Detyr staining represent paired images where the Tyr distal axon in (A) is from the same neuron as the Tyr cell body staining in (B) with the same true for Detyr. Representative paired images were chosen from more than four images per condition per experiment of similar quality.
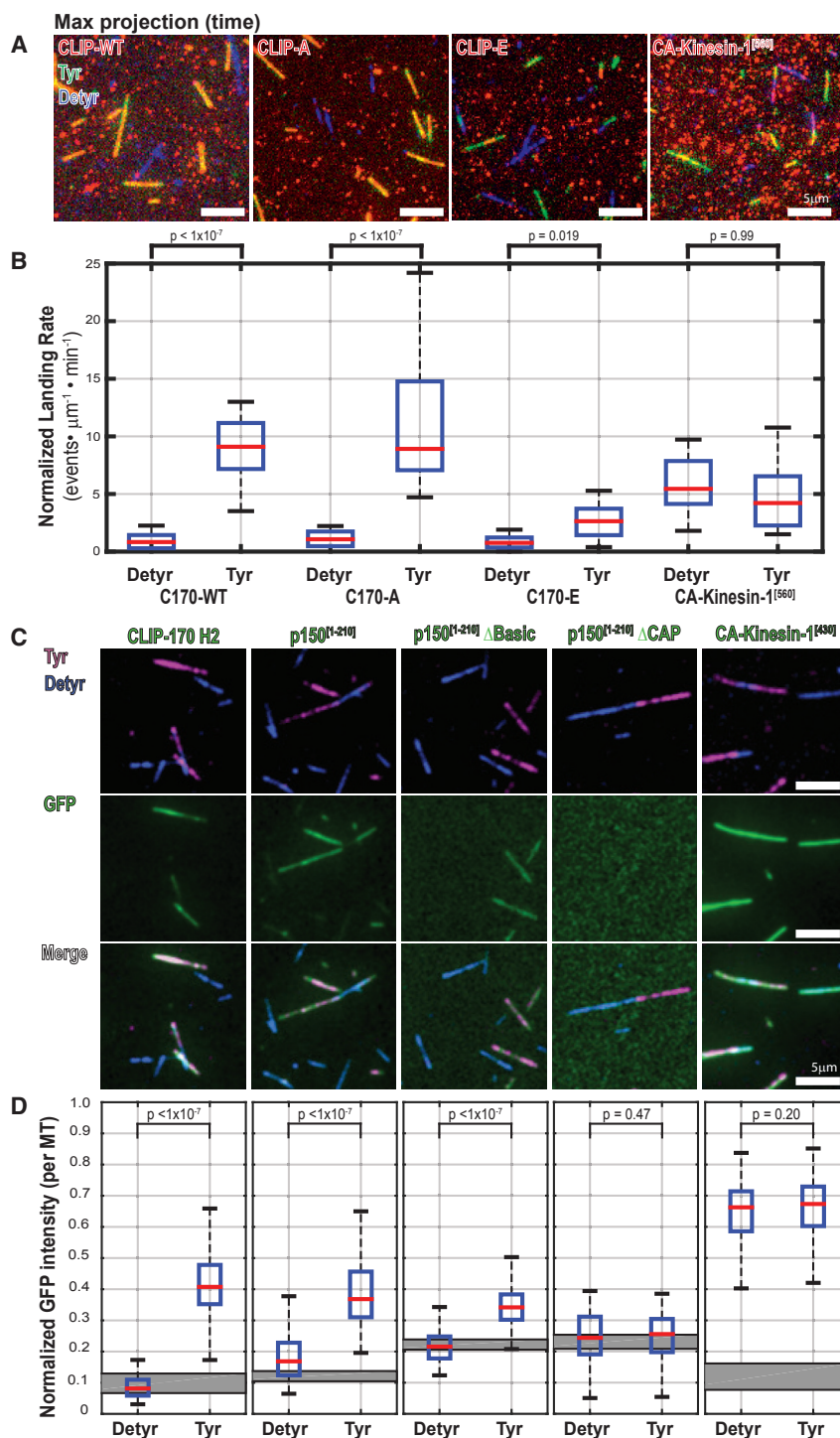
Figure 6. CLIP-170 Phosphorylation Regulates Recruitment to Tyr-Microtubules

(A) Image of maximum intensity projection over time shows selective localization of CLIP-WT and CLIP-A to Tyr microtubules. CLIP-E shows reduced localization to Tyr microtubules.

(B) Quantification of landing rate on Tyr- or Detyr-microtubules shows a significantly increased landing rate of CLIP-WT and CLIP-A on Tyr-microtubules. CLIP-E retains a significant preference for Tyr-microtubules, but landing is significantly reduced compared to CLIP-WT or CLIP-A (a table of all pairwise post-tests is found in Table S2). Single-molecule landing rates for CA-kinesin-1[560] in cell extracts show no differences between Tyr-/Detyr-microtubules (n > 24 movies per condition, each movie with >500 events; N = 3 independent cell lysate preparations; KW ANOVA with Tukey post-tests). The estimated final concentration of TMR-labeled HT-CLIP in this assay was ~0.5 nM for HT-CLIP constructs or 2.5 nM for CA-kinesin-1[560].

(C) Image panel for ensemble recruitment assay using 100 nM purified proteins. Faint GFP-p150[1–210] signal is present on Detyr microtubules and is likely mediated by the low-affinity basic microtubule binding domain.

(D) Quantification of the median normalized GFP fluorescent intensity per microtubule. The gray rectangle indicates the 95% CI for the median normalized GFP intensity for areas with no microtubules in each condition (n > 100 microtubules per condition; N = 3; KW ANOVA with Tukey post-tests). No exogenous EB1 was added in the experiments shown in Figures 6A–6D.

account for regional differences in transport at the cellular scale.

Second, layered regulatory interactions allow tuning of transport initiation that may be responsive to the specialized cytoskeletal architecture of differentiated cell types. For example, cells with sparse microtubules or slow rates of vesicle diffusion may exhibit distance-limited transport and rely on CLIP-170-dependent extension of the microtubule search radius to decrease diffusion distance. In contrast, cells with dense microtubule networks may exhibit capture-limited transport, relying on a spatially defined enrichment of tyrosinated tubulin to increase the binding efficiency of cargo within the microtubule search radius.

In the specific case of retrograde transport initiation in the neuron, high levels of Tyr-tubulin in the distal axon (Robson and Burgoyne, 1989; Brown et al., 1993) coincide with the region where many essential cargo and signaling factors initiate transport. Although we modeled LAMP1-positive vesicles here, all other cargoes we have examined require this mechanism for retrograde transport initiation, including Rab5-positive endosomes, TrkA/TrkB signaling endosomes, and mitochondria

preferentially recruit motor-cargo can account for cargo landing anywhere along the Tyr microtubule lattice, which extends the potential landing zone up to 20 μm from the axon tip, a much more extensive zone than the ~1 μm EB-comet tails at dynamic microtubule plus ends. Thus, spatial regulation of microtubule post-translational modifications may
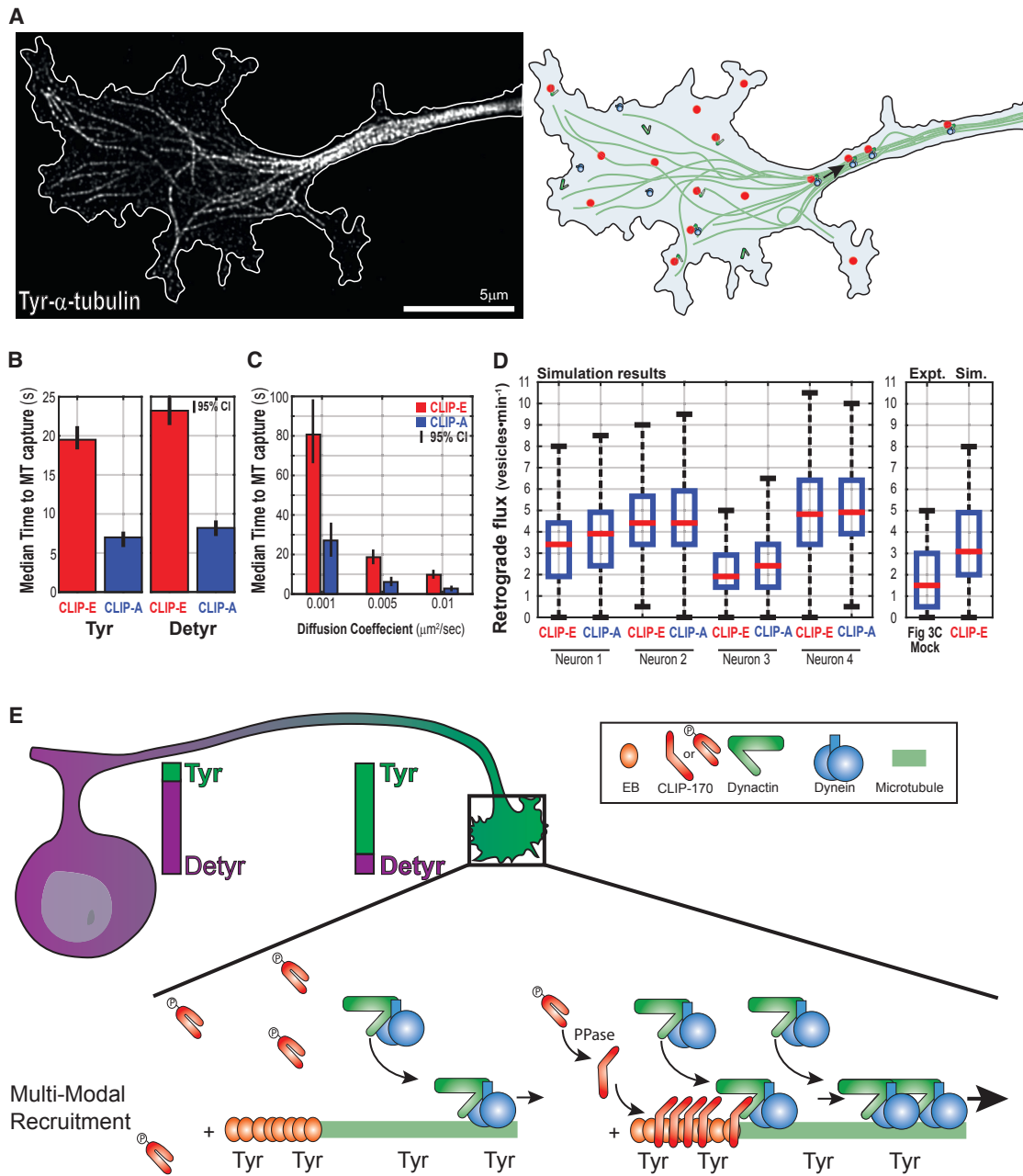
Figure 7. Simulation of Vesicle Diffusion and Microtubule Capture in the Distal Axon

(A) STED image Tyr-microtubules in the neuronal growth cone with the cell border outlined in white (left) and a schematic growth cone (right).

(B) Median (with bootstrapped 95% CI of the median) for the effective time to microtubule capture in computer simulations with CLIP-E or CLIP-A and either Tyr or Detyr binding probabilities (D = 0.006 μm^2/s).

(C) Median time to microtubule capture using Tyr binding probabilities and a range of diffusion coefficients (also see Figure S7).

(D) Simulated retrograde flux for four different traced neuronal growth cones used in the simulation. In some neurons, CLIP-A decoration increases the simulated retrograde flux. The boxplot to the right compares experimental results with the compiled simulation results for CLIP-E.

(E) Working model for the regulation of transport initiation in neurons. A gradient of tyrosinated α-tubulin is enriched in the distal axon provides spatial regulation and promotes efficient binding in a region where many cargos originate. CLIP-170 is highly phosphorylated and not microtubule associated in the growth cone at baseline. Transient or local dephosphorylation may provide temporal regulation and is required for efficient transport initiation in neurons.

(Moughamian et al., 2013). CLIP-170 contributes by extending the microtubule search radius in the growth cone, where microtubule density is low. This mechanism can be tightly regulated in time, as the phosphorylation state of CLIP-170 modulates auto-inhibition and thus allows for temporal tuning of the CLIP-170-dependent recruitment pathway. In combination, these

pathways give robust spatial and temporal control of transport initiation based on cellular needs.

CLIP-170 and Retrograde Transport Initiation

We propose that the distal pool of CLIP-170 is highly phosphorylated and thus preferentially assumes the closed conformation. The transient or local dephosphorylation of CLIP-170 would relieve autoinhibition and favor the open conformation that promotes efficient transport initiation. Recent large-scale phosphoproteomic studies in mammalian tissue indicate that CLIP-170 in brain is highly phosphorylated (Huttlin et al., 2010; Liao et al., 2012) and therefore autoinhibited. The predominance of autoinhibited CLIP-170 is consistent with recent immunofluorescent staining in the *Drosophila* and mammalian neuronal growth cones, where much of either D-CLIP-190 or CLIP-170 was found to be soluble or associated with F-actin patches (Beaven et al., 2015). Here, we show that dephosphorylation of CLIP-170 is likely to be an important and highly regulated step in the initiation of transport in the distal axon. However, CLIP-170 may do more than bind microtubules in the distal axon. For example, CLIP-170 interacts with the formin mDia1 (Lewkowicz et al., 2008) and may facilitate crosstalk between actin and microtubules. With respect to axonal transport, the enrichment of CLIP-170 in actin-rich regions of the growth cone suggests there may be a pathway to promote efficient translocation of actin-coated endosomes to microtubules for transport initiation.

Regulation of Transport by Post-translational Modifications

In the proposed model, post-translational modifications of microtubules and +TIPs work together to regulate transport initiation. Post-translational modifications of microtubules have received much attention recently, with a growing catalog of elements contributing to the "tubulin code" (Wehenkel and Janke, 2014; Yu et al., 2015). Here, we find a dramatic difference in the recruitment of organelles depending on the tyrosination state of α-tubulin. At the molecular level, CAP-Gly proteins such as p150[Glued] and CLIP-170 are highly sensitive to this modification (shown in Peris et al., 2006; Bieling et al., 2008; and this study), while kinesin-1 recruitment is insensitive to the tubulin tyrosination state in our assays, further demonstrating the specificity of the tubulin code. Additional support for a key role for α-tubulin detyrosination in regulating retrograde axonal transport comes from Song et al. (2015), who found that TTL is important for injury signaling after neuronal damage.

Why Do Cells Need Multiple Recruitment Mechanisms?

Although cells have evolved multiple mechanisms to promote robust transport initiation, it may not be immediately evident why the microtubule binding domains of motor proteins alone are not sufficient. Many kinesins are autoinhibited when not bound to microtubules, and thus it is not surprising that kinesin-dependent microtubule recruitment may require additional factors (Hirokawa et al., 2009). While cytosolic dynein is not known to be autoinhibited, recent structural work suggests potential autoinhibitory states (Torisawa et al., 2014). But even if dynein were not structurally autoinhibited, dynein's microtubule binding interactions are governed by nucleotide concentration,

and the high cellular ATP levels (~1 mM) (Rangaraju et al., 2014) favor the weak binding state of dynein (Porter and Johnson, 1983). These predictions agree with both biochemical and immunostaining observations that a significant fraction of dynein is cytosolic (Gill et al., 1991; Vaughan et al., 1999). Thus, motor-dependent recruitment alone may not be sufficient to explain the rapid and robust recruitment of motor-cargo complexes to microtubules in cells (Zajac et al., 2013).

Recruitment Mechanisms Promote Landing and Then Let Go

Both CLIP-A-dependent recruitment and Tyr-tubulin-dependent recruitment lead to an increased landing rate, without significant changes in the distribution of dwell times (Figures 2 and 5). This raises an interesting biophysical question as to how the apparent on-rate for cargo recruitment to the microtubule is increased while the off-rate or dwell time is unchanged. In the traditional theory of diffusion-controlled reactions, the reaction rate is governed by collision frequency and the on-rates do not change while the off-rates determine the duration of binding. However, this does not fit the observed data. One explanation may be that recruitment mechanisms change the spatial factor for the reaction by introducing multiple extended, flexible proteins such as p150[Glued] or CLIP-170 to increase the number and types of spatial conformations available for motor-mediated attachment. Importantly, the in vitro dwell time data agree with evidence from axonal transport studies in neurons, where the CAP-Gly domain of p150[Glued] is important for transport initiation in the distal axon, but it is not required to maintain sustained mid-axonal retrograde transport (Moughamian and Holzbaur, 2012; Moughamian et al., 2013). This suggests that although the p150[Glued] CAP-Gly must be accessible for microtubule recruitment, there is a mechanism to disengage the CAP-Gly domain so that it does not act as a brake to prevent sustained dynein motility (Ayloo et al., 2014). Recent structural work has shown that a subset of purified dynactin complexes have the N terminus of p150[Glued] folded back on itself, suggesting a structural conformation where the CAP-Gly domain is stably disengaged from the microtubule; however, the flexibility of this region made it difficult to visualize the CAP-Gly domain directly (Chowdhury et al., 2015; Urnavicius et al., 2015). The mechanism of disengagement and whether it occurs due to forces from dynein motility or requires additional protein adaptors remain to be determined.

Distinct Loading Mechanisms in the Distal Versus Mid-axon

We have previously shown that p150[Glued], CLIP-170, and EB1 are required for efficient distal transport initiation, but knockdown does not significantly affect mid-axonal transport (Moughamian and Holzbaur, 2012; Moughamian et al., 2013). Lis1, however, is a +TIP required for both distal and mid-axonal transport initiation (Moughamian et al., 2013). When Lis-1 binds to dynein, it induces a stable complex strongly bound to microtubules (Huang et al., 2012; Toropova et al., 2014). In the mid-axon, where teams of dynein mediate processive retrograde transport (Chowdary et al., 2015), individual motor detachment may be followed by Lis1 recruitment, leading to the formation of a stable motor-cargo-microtubule complex until transport can resume.

Lis1 then likely detaches from the motile dynein complexes, as observed in fungi (Egan et al., 2012; Lenz et al., 2006). However, the requirement of CLIP-170 for distal transport initiation in our assays indicates that mechanisms for Lis1-dependent initiation in fungi are insufficient to explain transport initiation in neurons.

Inefficient Transport Initiation Leads to Neurodegeneration

The importance of retrograde transport initiation in neurons is highlighted by the fact that mutations in p150^{Glued} that selectively disrupt transport initiation cause human neurodegeneration (Farrer et al., 2009; Moughamian and Holzbaur, 2012; Lloyd et al., 2012). Patients with mutations in the CAP-Gly domain develop Perry syndrome, a late-onset rapidly progressive and fatal parkinsonism (Wider and Wszolek, 2008). In addition, patients with nonsense mutations in CLIP-170 develop intellectual disability, seizures, and other complications (Larti et al., 2014). So what makes neurons especially vulnerable to reduced efficiency of transport initiation? First, a number of essential cargos initiate transport from the distal axon, including signaling endosomes carrying neurotrophic factors and autophagosomes (Cosker et al., 2008; Maday and Holzbaur, 2012). There is also a lower density of microtubules in the distal axon relative to the axon shaft, increasing the distance required for diffusion to microtubules. Further, decreased microtubule stability is associated with neurodegenerative diseases (Cartelli et al., 2012; Esteves et al., 2010), and tubulin tyrosine ligase expression may decrease with age (Gabius et al., 1983); these changes are predicted to further decrease binding efficiency. Importantly, the mechanisms regulating transport initiation described here suggest potential therapeutic approaches. Modulating either α-tubulin tyrosination or CLIP-170 activation may boost transport initiation and thus mitigate transport defects. However, "more is better" is not the simple motto for retrograde transport initiation, as the disease, cellular context, and specific cargo being transported make all the difference (Perlson et al., 2010).

EXPERIMENTAL PROCEDURES

Animal Work
All animal protocols were approved by the University of Pennsylvania institutional animal care and use committee.

Protein Biochemistry
Tyrosinated tubulin was purified from HeLa S3 cells (CCL-2.2; ATCC) as described previously (Barisic et al., 2015). Carboxypeptidase A (CPA; C9268, apparent 6 U/mg tubulin; Sigma) was added to the soluble tubulin to produce detyrosinated tubulin and the tyrosination status of the tubulin was verified by western blot (Figure 5B). See Supplemental Experimental Procedures for additional information.

In Vitro Reconstitution of Microtubule Recruitment
Double-cycled GMPCPP microtubules were polymerized according to Gell et al. (2010) using with 5% labeled tubulin (Alexa 488, Alexa Fluor 647, or TRITC; Cytoskeleton) and 95% unlabeled tubulin (bovine brain or HeLa tubulin). Cell lysates from COS-7 cells (CRL-1651; ATCC) were prepared as follows: cells expressed recombinant HaloTag constructs for ~22 hr, labeled with TMR-Halo ligand (Promega), and then lysed in 40 mM HEPES, 120 mM NaCl, 0.1% Triton X-100 supplemented with protease inhibitors (2 mM phenylmethylsulfonyl fluoride, 53 μM p-Tosyl arginine methyl ester, 210 μM leupeptin, and 1.5 μM pepstatin-A). Lysates were clarified by centrifugation at 17,000 × g

and again at 352,000 × g to obtain HSS. The relative concentration of TMR-labeled protein in cell extracts was determined by measuring the absorbance of TMR at 555 nm in reference to a standard curve of TMR at known concentrations. EGTA and EDTA were excluded from all buffers to maintain the integrity of the CLIP-170 Zn knuckle.

Motility assays were performed in flow chambers made from silanized (PlusOne Silane; GE) #1.5 coverslips (Warner) attached to glass slides using adhesive tape and vacuum grease. Typical chamber volumes were ~15 μl, incubation times were 5 min, and chambers were washed with three to four chamber volumes between incubations. Following incubation with monoclonal anti-β-tubulin (T5201; Sigma) diluted 1:200 in motility assay buffer (MAB; 10 mM PIPES, 50 mM K-acetate, and 4 mM MgCl$_2$ [pH 7.0]) and blocking with 5% pluronic F-127, labeled GMPCPP-stabilized microtubules were introduced, and chambers were pre-incubated with MAB supplemented with 0.3 mg/ml BSA, 0.3 mg/ml casein, 1 mM ATP, 15 mg/ml D-glucose, and 10 mM DTT; this buffer with supplements also served as the "assay buffer" for all in vitro assays except Figures 6C and 6D, where purified CA-kinesin-1 was supplemented with 1 mM AMP-PNP and no ATP was added to purified proteins. Vesicles diluted in assay buffer were added as noted with or without cell extract and unlabeled EB1, followed by an oxygen scavenging system (0.5 mg/ml glucose oxidase, 470 U/ml catalase, and 15mg/ml glucose). All assays with labeled Tyr or Detyr microtubules included an approximately equal number of repeats with the fluorescent label for Tyr or Detyr reversed (Figures S5B–S5D).

Vesicles were isolated from B6.SJL.Tg-(Thy1.2-p50-EGFP) mice (Ross et al., 2006), as described previously (Hendricks et al., 2014). See Supplemental Experimental Procedures for more information.

Cell Culture and Live-Cell Imaging
Dorsal root ganglia were dissected from adult WT mice, isolated, transfected using Amaxa Nucleofector SCN program 6 (Lonza), and cultured for 4 days in vitro (DIV) (Moughamian and Holzbaur, 2012; Perlson et al., 2009). Live-cell photobleaching and imaging of distal retrograde transport initiation was performed according to Nirschl and Holzbaur (2016). See Supplemental Experimental Procedures for more information.

All CLIP-170 knockdown and rescue neurons used for live-cell imaging experiments met the following criteria: low expression of recombinant HT-CLIP-170 protein; axonal processes extending >500 μm from the cell body; normal axonal contours and morphology with no swellings, bulbs, or membrane blebbing; and normal mid-axonal LAMP-1-RFP transport (as shown in Moughamian et al., 2013).

COS7 cells were cultured in DMEM supplemented with 10% fetal bovine serum and 1% L-glutamine. Cells at ~80% confluence were transfected using FuGENE6 (Roche).

For immunofluorescence, Cos7 cells were fixed in 4% paraformaldehyde (PFA) and neurons were fixed with 4% PFA/sucrose for 10 min. Cells were permeabilized with 0.2% Triton X-100 in PBS for 15 min, blocked, and incubated with primary antibodies overnight at 4C, then secondary antibody for 1 hr at room temperature. Samples were mounted in Mowiol-488 (Calbiochem).

Image Processing and Analysis
Particle tracking of TIRF images was performed in MATLAB R2015a using the open-source uTrack package (v.2.1.3) from the Danuser lab (Jaqaman et al., 2008). An initial parameter sweep was conducted to find the optimal uTrack parameters for detecting local maxima, multi-Gaussian fitting, track linking, and gap closing (Figure S4). See Supplemental Experimental Procedures for more information.

Distal Flux Image Analysis
Kymographs of LAMP-1-RFP transport initiation were prepared using the Kymograph Clear 1.0 ImageJ plugin (https://sites.google.com/site/kymographanalysis/version-information). Using the mask of the bleached region, a line was automatically generated 50 pixels (~3.5 μm) retrograde to the distal end of the bleached region for retrograde flux analysis. A vesicle counted in the flux measurement if it started distal to the bleached region and moved retrograde 3.5 μm through the site of flux measurement, regardless of later directional reversals. The number of vesicles crossing the flux line was manually counted for every neuron, with the analyst blinded to experimental condition.

Movies S2, S3, and S4 were processed with the ImageJ (NIH) background subtraction plugin (rolling ball, 20-pixel radius) for improved visualization. However, all TIRF particle tracking and analysis was performed on raw, unprocessed data. Individual line scans in Figure 4 were drawn along the β-tubulin image; Tyr or Detyr intensity along this line was normalized to β-tubulin intensity for each image, and the normalized Tyr/Detyr ratio was smoothed with a sliding window mean filter prior to calculating the bootstrapped mean and 95% CI intensity values. Microtubule images in Figure 6 were background subtracted using the method above for visual clarity. The GFP intensity images (Figure 6C) for measuring fluorescent intensity were filtered with a Gaussian kernel to reduce the contribution of high-frequency noise. Where specified, images were deconvolved using Huygens Professional.

Simulation of Vesicle Diffusion and Microtubule Capture in the distal axon

Computer simulations were performed as described in the results section. Pseudocode for the simulation of vesicle diffusion and microtubule capture is shown in Figure S7A. See Supplemental Experimental Procedures for more information.

Statistics

Statistical tests and distribution fitting were performed in MATLAB R2015a, as noted in the legends. Box and whisker plots show the median (red bar) and interquartile range (IQR; blue box) with whiskers extending to the most extreme inliers. Statistical outliers, defined as data greater than median × 1.5*IQR, were included in all analysis but are not shown in boxplots to avoid compression of the majority of data. Statistical abbreviations are as follows: n, number of observations per condition, per experiment; N, number of independent experiments. See Supplemental Experimental Procedures for more information.

SUPPLEMENTAL INFORMATION

Supplemental Information includes Supplemental Experimental Procedures, seven figures, two tables, and four movies and can be found with this article online at http://dx.doi.org/10.1016/j.celrep.2016.02.046.

REFERENCES

Akhmanova, A., and Steinmetz, M.O. (2008). Tracking the ends: a dynamic protein network controls the fate of microtubule tips. Nat. Rev. Mol. Cell Biol. 9, 309–322.

Alushin, G.M., Lander, G.C., Kellogg, E.H., Zhang, R., Baker, D., and Nogales, E. (2014). High-resolution microtubule structures reveal the structural transitions in αβ-tubulin upon GTP hydrolysis. Cell 157, 1117–1129.

Ayloo, S., Lazarus, J.E., Dodda, A., Tokito, M., Ostap, E.M., and Holzbaur, E.L. (2014). Dynactin functions as both a dynamic tether and brake during dynein-driven motility. Nat. Commun. 5, 4807.

Barisic, M., Silva e Sousa, R., Tripathy, S.K., Magiera, M.M., Zaytsev, A.V., Pereira, A.L., Janke, C., Grishchuk, E.L., and Maiato, H. (2015). Mitosis. Microtubule detyrosination guides chromosomes during mitosis. Science 348, 799–803.

Beaven, R., Dzhindzhev, N.S., Qu, Y., Hahn, I., Dajas-Bailador, F., Ohkura, H., and Prokop, A. (2015). Drosophila CLIP-190 and mammalian CLIP-170 display reduced microtubule plus end association in the nervous system. Mol. Biol. Cell 26, 1491–1508.

Bieling, P., Kandels-Lewis, S., Telley, I.A., van Dijk, J., Janke, C., and Surrey, T. (2008). CLIP-170 tracks growing microtubule ends by dynamically recognizing composite EB1/tubulin-binding sites. J. Cell Biol. 183, 1223–1233.

Brown, A., Li, Y., Slaughter, T., and Black, M.M. (1993). Composite microtubules of the axon: quantitative analysis of tyrosinated and acetylated tubulin along individual axonal microtubules. J. Cell Sci. 104, 339–352.

Cartelli, D., Goldwurm, S., Casagrande, F., Pezzoli, G., and Cappelletti, G. (2012). Microtubule destabilization is shared by genetic and idiopathic Parkinson's disease patient fibroblasts. PLoS ONE 7, e37467.

Chowdary, P.D., Che, D.L., Zhang, K., and Cui, B. (2015). Retrograde NGF axonal transport—motor coordination in the unidirectional motility regime. Biophys. J. 108, 2691–2703.

Chowdhury, S., Ketcham, S.A., Schroer, T.A., and Lander, G.C. (2015). Structural organization of the dynein-dynactin complex bound to microtubules. Nat. Struct. Mol. Biol. 22, 345–347.

Cosker, K.E., Courchesne, S.L., and Segal, R.A. (2008). Action in the axon: generation and transport of signaling endosomes. Curr. Opin. Neurobiol. 18, 270–275.

Dixit, R., Barnett, B., Lazarus, J.E., Tokito, M., Goldman, Y.E., and Holzbaur, E.L. (2009). Microtubule plus-end tracking by CLIP-170 requires EB1. Proc. Natl. Acad. Sci. USA 106, 492–497.

Duellberg, C., Trokter, M., Jha, R., Sen, I., Steinmetz, M.O., and Surrey, T. (2014). Reconstitution of a hierarchical +TIP interaction network controlling microtubule end tracking of dynein. Nat. Cell Biol. 16, 804–811.

Egan, M.J., Tan, K., and Reck-Peterson, S.L. (2012). Lis1 is an initiation factor for dynein-driven organelle transport. J. Cell Biol. 197, 971–982.

Ersfeld, K., Wehland, J., Plessmann, U., Dodemont, H., Gerke, V., and Weber, K. (1993). Characterization of the tubulin-tyrosine ligase. J. Cell Biol. 120, 725–732.

Esteves, A.R., Arduíno, D.M., Swerdlow, R.H., Oliveira, C.R., and Cardoso, S.M. (2010). Microtubule depolymerization potentiates alpha-synuclein oligomerization. Front Aging Neurosci 1, 5.

Farrer, M.J., Hulihan, M.M., Kachergus, J.M., Dächsel, J.C., Stoessl, A.J., Grantier, L.L., Calne, S., Calne, D.B., Lechevalier, B., Chapon, F., et al. (2009). DCTN1 mutations in Perry syndrome. Nat. Genet. 41, 163–165.

Gabius, H.-J., Graupner, G., and Cramer, F. (1983). Activity patterns of aminoacyl-tRNA synthetases, tRNA methylases, arginyltransferase and tubulin:tyrosine ligase during development and ageing of Caenorhabditis elegans. Eur. J. Biochem. 131, 231–234.

Galjart, N. (2005). CLIPs and CLASPs and cellular dynamics. Nat. Rev. Mol. Cell Biol. 6, 487–498.

Gell, C., Bormuth, V., Brouhard, G.J., Cohen, D.N., Diez, S., Friel, C.T., Helenius, J., Nitzsche, B., Petzold, H., Ribbe, J., et al. (2010). Microtubule dynamics reconstituted in vitro and imaged by single-molecule fluorescence microscopy. Methods Cell Biol. 95, 221–245.

Gill, S.R., Schroer, T.A., Szilak, I., Steuer, E.R., Sheetz, M.P., and Cleveland, D.W. (1991). Dynactin, a conserved, ubiquitously expressed component of an activator of vesicle motility mediated by cytoplasmic dynein. J. Cell Biol. 115, 1639–1650.

Hendricks, A.G., Perlson, E., Ross, J.L., Schroeder, H.W., 3rd, Tokito, M., and Holzbaur, E.L. (2010). Motor coordination via a tug-of-war mechanism drives bidirectional vesicle transport. Curr. Biol. 20, 697–702.

Hendricks, A.G., Goldman, Y.E., and Holzbaur, E.L. (2014). Reconstituting the motility of isolated intracellular cargoes. Methods Enzymol. 540, 249–262.

Hirokawa, N., Noda, Y., Tanaka, Y., and Niwa, S. (2009). Kinesin super-family motor proteins and intracellular transport. Nat. Rev. Mol. Cell Biol. 10, 682–696.

Huang, J., Roberts, A.J., Leschziner, A.E., and Reck-Peterson, S.L. (2012). Lis1 acts as a "clutch" between the ATPase and microtubule-binding domains of the dynein motor. Cell 150, 975–986.

Huttlin, E.L., Jedrychowski, M.P., Elias, J.E., Goswami, T., Rad, R., Beausoleil, S.A., Villén, J., Haas, W., Sowa, M.E., and Gygi, S.P. (2010). A tissue-specific atlas of mouse protein phosphorylation and expression. Cell 143, 1174–1189.

Janke, C., and Kneussel, M. (2010). Tubulin post-translational modifications: encoding functions on the neuronal microtubule cytoskeleton. Trends Neurosci. 33, 362–372.

Jaqaman, K., Loerke, D., Mettlen, M., Kuwata, H., Grinstein, S., Schmid, S.L., and Danuser, G. (2008). Robust single-particle tracking in live-cell time-lapse sequences. Nat. Methods 5, 695–702.

Kreitzer, G., Liao, G., and Gundersen, G.G. (1999). Detyrosination of tubulin regulates the interaction of intermediate filaments with microtubules in vivo via a kinesin-dependent mechanism. Mol. Biol. Cell 10, 1105–1118.

Kumar, N., and Flavin, M. (1981). Preferential action of a brain detyrosinolating carboxypeptidase on polymerized tubulin. J. Biol. Chem. 256, 7678–7686.

Lansbergen, G., Komarova, Y., Modesti, M., Wyman, C., Hoogenraad, C.C., Goodson, H.V., Lemaitre, R.P., Drechsel, D.N., van Munster, E., Gadella, T.W., Jr., et al. (2004). Conformational changes in CLIP-170 regulate its binding to microtubules and dynactin localization. J. Cell Biol. 166, 1003–1014.

Larti, F., Kahrizi, K., Musante, L., Hu, H., Papari, E., Fattahi, Z., Bazazzadegan, N., Liu, Z., Banan, M., Garshasbi, M., et al. (2014). A defect in the CLIP1 gene (CLIP-170) can cause autosomal recessive intellectual disability. Eur. J. Hum. Genet. 23, 331–336.

Lee, H.S., Komarova, Y.A., Nadezhdina, E.S., Anjum, R., Peloquin, J.G., Schober, J.M., Danciu, O., van Haren, J., Galjart, N., Gygi, S.P., et al. (2010). Phosphorylation controls autoinhibition of cytoplasmic linker protein-170. Mol. Biol. Cell 21, 2661–2673.

Lenz, J.H., Schuchardt, I., Straube, A., and Steinberg, G. (2006). A dynein loading zone for retrograde endosome motility at microtubule plus-ends. 25, 2275–2286.

Lewkowicz, E., Herit, F., Le Clainche, C., Bourdoncle, P., Perez, F., and Niedergang, F. (2008). The microtubule-binding protein CLIP-170 coordinates mDia1 and actin reorganization during CR3-mediated phagocytosis. J. Cell Biol. 183, 1287–1298.

Liao, L., Sando, R.C., III, Farnum, J.B., Vanderklish, P.W., Maximov, A., and Yates, J.R., III. (2012). 15 N-labeled brain enables quantification of proteome and phosphoproteome in cultured primary neurons. J Proteome Res. 11, 1341–1353.

Lloyd, T.E., Machamer, J., O'Hara, K., Kim, J.H., Collins, S.E., Wong, M.Y., Sahin, B., Imlach, W., Yang, Y., Levitan, E.S., et al. (2012). The p150(Glued) CAP-Gly domain regulates initiation of retrograde transport at synaptic termini. Neuron 74, 344–360.

Lomakin, A.J., Semenova, I., Zaliapin, I., Kraikivski, P., Nadezhdina, E., Slepchenko, B.M., Akhmanova, A., and Rodionov, V. (2009). CLIP-170-dependent capture of membrane organelles by microtubules initiates minus-end directed transport. Dev. Cell 17, 323–333.

Lopez, B.J., and Valentine, M.T. (2015). The +TIP coordinating protein EB1 is highly dynamic and diffusive on microtubules, sensitive to GTP analog, ionic strength, and EB1 concentration. Cytoskeleton (Hoboken) 73, 23–34.

Maday, S., and Holzbaur, E.L. (2012). Autophagosomes initiate distally and mature during transport toward the cell soma in primary neurons. J. Cell Biol. 196, 407–417.

Maday, S., Twelvetrees, A.E., Moughamian, A.J., and Holzbaur, E.L. (2014). Axonal transport: cargo-specific mechanisms of motility and regulation. Neuron 84, 292–309.

Moughamian, A.J., Osborn, G.E., Lazarus, J.E., Maday, S., and Holzbaur, E.L. (2013). Ordered recruitment of dynactin to the microtubule plus-end is required for efficient initiation of retrograde axonal transport. J. Neurosci. 33, 13190–13203.

Moughamian, A.J., and Holzbaur, E.L. (2012). Dynactin is required for transport initiation from the distal axon. Neuron 74, 331–343.

Nirschl, J.J., and Holzbaur, E.L. (2016). Live-cell imaging of retrograde transport initiation in primary neurons. Biophys. Methods Cell Biol. 131, 269–276.

Peris, L., Thery, M., Fauré, J., Saoudi, Y., Lafanechère, L., Chilton, J.K., Gordon-Weeks, P., Galjart, N., Bornens, M., Wordeman, L., et al. (2006). Tubulin tyrosination is a major factor affecting the recruitment of CAP-Gly proteins at microtubule plus ends. J. Cell Biol. 174, 839–849.

Perlson, E., Jeong, G.B., Ross, J.L., Dixit, R., Wallace, K.E., Kalb, R.G., and Holzbaur, E.L. (2009). A switch in retrograde signaling from survival to stress in rapid-onset neurodegeneration. J. Neurosci. 29, 9903–9917.

Perlson, E., Maday, S., Fu, M.M., Moughamian, A.J., and Holzbaur, E.L. (2010). Retrograde axonal transport: pathways to cell death? Trends Neurosci. 33, 335–344.

Pierre, P., Scheel, J., Rickard, J.E., and Kreis, T.E. (1992). CLIP-170 links endocytic to microtubules. Cell 70, 887–900.

Porter, M.E., and Johnson, K.A. (1983). Of the ATP-induced dissociation of the dynein-microtubule complex. J. Biol. Chem. 258, 6582–6587.

Prota, A.E., Magiera, M.M., Kuijpers, M., Bargsten, K., Frey, D., Wieser, M., Jaussi, R., Hoogenraad, C.C., Kammerer, R.A., Janke, C., and Steinmetz, M.O. (2013). Structural basis of tubulin tyrosination by tubulin tyrosine ligase. J. Cell Biol. 200, 259–270.

Rangaraju, V., Calloway, N., and Ryan, T.A. (2014). Activity-driven local ATP synthesis is required for synaptic function. Cell 156, 825–835.

Rickard, J.E., and Kreis, T.E. (1996). CLIPS for organelle-microtubule interactions. Trends Cell Biol. 6, 178–183.

Rickard, J.E., and Kreis, T.E. (1991). Binding of pp170 to microtubules is regulated by phosphorylation. J. Biol. Chem. 266, 17597–17605.

Robson, S.J., and Burgoyne, R.D. (1989). Differential localisation of tyrosinated, detyrosinated, and acetylated alpha-tubulins in neurites and growth cones of dorsal root ganglion neurons. Cell Motil. Cytoskeleton 12, 273–282.

Ross, J.L., Wallace, K., Shuman, H., Goldman, Y.E., and Holzbaur, E.L. (2006). Processive bidirectional motion of dynein-dynactin complexes in vitro. Nat. Cell Biol. 8, 562–570.

Scheel, J., Pierre, P., Rickard, J.E., Diamantopoulos, G.S., Valetti, C., van der Goot, F.G., Häner, M., Aebi, U., and Kreis, T.E. (1999). Purification and analysis of authentic CLIP-170 and recombinant fragments purification and analysis of authentic cLIP-170 and recombinant fragments. J. Biol. Chem. 274, 25883–25891.

Song, W., Cho, Y., Watt, D., and Cavalli, V. (2015). Tubulin-tyrosine ligase (TTL)-mediated increase in tyrosinated α-tubulin in injured axons is required for retrograde injury signaling and axon regeneration. J. Biol. Chem. 290, 4765–4775.

Torisawa, T., Ichikawa, M., Furuta, A., Saito, K., Oiwa, K., Kojima, H., Toyoshima, Y.Y., and Furuta, K. (2014). Autoinhibition and cooperative activation mechanisms of cytoplasmic dynein. Nat. Cell Biol. 16, 1118–1124.

Toropova, K., Zou, S., Roberts, A.J., Redwine, W.B., Goodman, B.S., Reck-Peterson, S.L., and Leschziner, A.E. (2014). Lis1 regulates dynein by sterically blocking its mechanochemical cycle. eLife 3, e03372.

Urnavicius, L., Zhang, K., Diamant, A.G., Motz, C., Schlager, M.A., Yu, M., Patel, N.A., Robinson, C.V., and Carter, A.P. (2015). The structure of the dynactin complex and its interaction with dynein. Science 347, 1441–1446.

Vaughan, K.T. (2005). Microtubule plus ends, motors, and traffic of Golgi membranes. Biochim. Biophys. Acta 1744, 316–324.

Vaughan, K.T., Tynan, S.H., Faulkner, N.E., Echeverri, C.J., and Vallee, R.B. (1999). Colocalization of cytoplasmic dynein with dynactin and CLIP-170 at microtubule distal ends. J. Cell Sci. *112*, 1437–1447.

Watson, P., and Stephens, D.J. (2006). Microtubule plus-end loading of p150(Glued) is mediated by eb1 and clip-170 but is not required for intracellular membrane traffic in mammalian cells. J. Cell Sci. *119*, 2758–2767.

Wehenkel, A., and Janke, C. (2014). Towards elucidating the tubulin code. Nat. Cell Biol. *16*, 303–305.

Weisbrich, A., Honnappa, S., Jaussi, R., Okhrimenko, O., Frey, D., Jelesarov, I., Akhmanova, A., and Steinmetz, M.O. (2007). Structure-function relationship of CAP-Gly domains. Nat Struct Mol Biol. *14*, 959–967.

Wider, C., and Wszolek, Z.K. (2008). Rapidly progressive familial parkinsonism with central hypoventilation, depression and weight loss (Perry syndrome)—a literature review. Parkinsonism Relat. Disord. *14*, 1–7.

Yu, I., Garnham, C.P., and Roll-Mecak, A. (2015). Writing and reading the tubulin code. J. Biol. Chem. *290*, 17163–17172.

Zajac, A.L., Goldman, Y.E., Holzbaur, E.L., and Ostap, E.M. (2013). Local cytoskeletal and organelle interactions impact molecular-motor- driven early endosomal trafficking. Curr. Biol. *23*, 1173–1180.

Zanic, M., Stear, J.H., Hyman, A.A., and Howard, J. (2009). EB1 recognizes the nucleotide state of tubulin in the microtubule lattice. PLoS ONE *4*, e7585.